PERGAMON

International Journal of Heat and Mass Transfer 44 (2001) 1401–1410

International Journal of HEAT and MASS TRANSFER

www.elsevier.com/locate/ijhmt

Radiation effects on mixed convection heat transfer in a vertical square duct

Wei-Mon Yan *, Hung-Yi Li

Department of Mechanical Engineering, Huafan Institute of Technology, Huafan University, Shih Ting, Taipei 22305, Taiwan, ROC

Received 22 July 1999; received in revised form 28 April 2000

Abstract

A numerical study has been made of the interaction of the thermal radiation with laminar mixed convection for a gray fluid (a gas that may have particulates in suspension) in a vertical square duct. Using the vorticity-velocity method, the three-dimensional Navier–Stokes equations and energy equations were solved simultaneously. The integro-differential radiative transfer equation was solved by the discrete ordinates method. Results are presented for a wide range of governing parameters. The effects are emphasized of thermal buoyancy and radiative transfer on the development of velocity and temperature fields, the friction factor and the Nusselt number. The results show that radiation significantly affects the total Nusselt number Nu_t and tends to reduce the buoyancy effects. In addition, radiation speeds the development of the temperature field.

1. Introduction

Mixed convection in a vertical duct has been of special interest recently due to applications such as solar collectors, heat exchangers, nuclear reactors and electronic equipment. When convection and radiation effects are of similar importance, separate calculation of these and superposition without considering their interaction can result in signficant errors. The momentum, energy and radiation transport equations in such cases should be solved simultaneously in order to accurately determine the velocity and temperature fields and heat transfer rates. The present work addresses this problem.

Much work, both theoretical and experimental, has been done on mixed-convection heat transfer in internal flows, as is evident in the review by Jackson et al. [1]. Publications relevant to the present work are briefly reviewed here. Mixed convection heat transfer between vertical parallel plates has been studied by many researchers [2–7]. Aung and Worku [2] show that the hydrodymanic entry length first increases rapidly with Gr/Re and then approaches an asymptotic value at large Gr/Re. Habchi and Acharya [5] find the local Nusselt number to increase with increasing value Gr/Re^2. Ingham et al. [7] present a numerical method to treat the flow reversal in buoyancy-assisting and -opposing flows. They predict poor heat transfer when flow is retarded by opposed buoyancy, but at large and negative Gr/Re heat transfer is quite effective.

In flow with low Peclet number or high buoyancy effect, flow reversal may occur. Recently, this case was studied for flows between vertical parallel plates [8–11] or in vertical tubes [12–14]. It appears that at low Peclet number, the omission of axial diffusion terms in the momentum and energy equations leads to serious errors. However, at $Pe > 50$, the matching technique used with the boundary-layer equations produces accurate predictions of heat transfer along the heated wall.

Analytical solutions of fully developed mixed convection in vertical rectangular ducts with different heating conditions are presented by Igbal and Aggarwala [15] and Cheng and Weng [16]. They examined in detail the physical conditions for flow. In practice, the flow typically remains in development for almost the

* Corresponding author. Tel.: +886-2-26632102 extn: 4038; fax: +886-2-26633847.

E-mail address: wmyan@huafan.hfu.edu.tw (W.-M. Yan).

0017-9310/01/$ - see front matter
PII: S0017-9310(00)00148-4

Nomenclature

a	width of a square duct, m
f	friction factor, $2\overline{\tau}_w/(\rho w_o^2)$
G, G^*	dimensional and dimensionless incident radiation, $G^* = G/(4\overline{n}^2\sigma T_w^4)$
Gr	Grashof number, $g\beta(T_w - T_o)a^3/v^2$
$\overline{h}$	circumferentially averaged heat transfer coefficient, W/m^2K
k	thermal conductivity, W/m k
m, m'	direction of the discrete ordinates
M, N	number of finite difference divisions in the X and Y directions, respectively
n	direction coordinate normal to the duct wall
$\overline{n}$	refractive index
N^*	order of the phase function
N_c	conduction-to-radiation parameter, $k\kappa/(4\overline{n}^2\sigma T_w^3)$
Nu_c	connective Nusselt number
Nu_r	radiative Nusselt number
Nu_t	total Nusselt number, $Nu_t = Nu_c + Nu_r$
p, P	dimensional and dimensionless pressure, respectively
$\overline{p}$	cross-sectional mean pressure, Pa
$\overline{P}$	dimensionless cross-sectional mean pressure
P'	perturbation term about the mean pressure $\overline{P}$
Pe	Peclet number, $Pr \cdot Re$
P_n	Legendre polynomial
P_r	Prandtl number, v/α
$\vec{q}_c$	convective heat flux
$\vec{q}_r$	radiation heat flux
$\vec{q}_t$	total heat flux
$\vec{Q}_r$	dimensionless radiation flux
Ra	Rayleigh number $Pr \cdot Gr$
Re	Reynolds number, $w_o a/v$
T	temperature, K
u, v, w	velocity components in x, y and z directions, respectively, m/s
U, V, W	dimensionless velocity components in X, Y and Z directions, respectively
w_o	inlet mean velocity, m/s
x, y, z	rectangular coordinate, m
X, Y, Z	dimensionless rectangular coordinate, $X = x/a$, $Y = y/a$, $Z = z/(a \cdot Re)$
Z^*	dimensionless coordinate in the z direction, $Z^* = Z/Pr$
∇^*	dimensionless gradient operator

Greek symbols

α	thermal diffusivity, m^2/s
β	coefficient of thermal expansion
κ	extinction coefficient, m^{-1}
κ_S	scattering coefficient, m^{-1}
ϵ_w	wall emissivity
θ	dimensionless temperature, T/T_w
θ_o	dimensionless temperature ratio, T_o/T_w
μ, η, ζ	direction cosines
v	kinematic viscosity, m^2/s
ξ	dimensionless vorticity in axial direction, $\partial U/\partial Y - \partial V/\partial X$
ρ	density, kg/m^3
σ	Stefan–Boltzman constant, $5.67 \times 10^{-8} W/m^2\ K^{-4}$
τ	optical thickness
τ_w	wall shear stress, kPa
ψ	dimensionless radiation intensity, $\pi I/(\overline{n}^2\sigma T_w^4)$
ϕ	scattering phase function
ω	single scattering albedo
$\vec{\Omega}, \vec{\Omega}'$	outward and inward direction of radiation
Ω	solid angle

Subscripts

b	bulk fluid quantity
c	convective
o	condition at inlet
r	radiative
w	value at wall

Superscript

$\overline{\ }$	averaged value

full length of the duct, so a knowledge of the developing mixed convection is important. Cheng and Weng [17] present relevant numerical results of developing mixed convection heat transfer in vertical rectangular ducts without consideration of the thermal radiation effects.

Forced convection in a channel with radiation effect only (i.e., without thermal buoyancy) has been examined by several investigators [18–24] during the past thirty years for ducts with a prescribed heat flux or wall temperature distribution on the wall surfaces. In these studies, various approximate methods were used for radiative transport in the medium (the flowing fluid). Among these, the differential approximation methods describe approximation variation of the intensity of radiation as function of position and angle.

No numerical studies have been published of combined convection and radiation in mixed convection duct flows. This motivates the present study. In addition, flow is considered to be hydrodynamically and thermally developing.

2. Analysis

As a preliminary attempt to study thermal radiation effects, flow is assumed to be laminar. Practical flows are, of course, often turbulent. Accounting for turbulence, however, greatly complicates the simulation. The present work is thus a first step.

Consider, therefore, steady laminar flow through a vertical square duct of width a and uniform wall Temperature T_w. A uniform inlet axial velocity w_o and a uniform inlet temperature T_o are imposed at the entrance $z = 0$. The u, v, and w are the velocity components in the x, y, and z directions, respectively. To simplify analysis, the fluid properties are taken to be constants expect for the density variation in the buoyancy term of the momentum equation. The Boussinesq approximation is invoked for the thermal buoyancy effect. The viscous dissipation and compression effects in the energy equation are negligible due to low Mach number flows. Additionally, the gas is assumed to be gray, absorbing, emitting, and scattering.

The flow is treated as parabolic and a space-averaged pressure $\overline{p}$ is imposed in the momentum equations to prevail at each cross-section, thus permitting a decoupling from the pressure p_m in the cross-stream momentum equations. This "pressure uncoupling" follows the parabolic-flow practice and, together with the assumption that neither momentum nor heat is diffused in the axial direction (supported by an order of magnitude analysis), permits a marching-integration calculation procedure [25]. To conveniently present the governing equations, the pressure p can be represented as the sum of a cross-section mean pressure $\overline{p}(z)$, which drives the main flow, and a perturbation about the mean, $p'(x,y,z)$, which drives the cross-stream flow,

$$p = \overline{p}(z) + p'(x,y,z). \tag{1}$$

By introducing a vorticity function in the axial direction, $\xi = \partial U/\partial Y - \partial V/\partial X$, the vorticity–velocity formulation of Navier–Stokes equations is obtained:

$$\partial^2 U/\partial X^2 + \partial^2 U/\partial Y^2 = \partial\xi/\partial Y - \partial^2 W/\partial X\partial Z, \tag{2}$$

$$\partial^2 V/\partial X^2 + \partial^2 V/\partial Y^2 = -\partial\xi/\partial X - \partial^2 W/\partial Y\partial Z, \tag{3}$$

$$\begin{aligned} U\partial\xi/\partial X + V\partial\xi/\partial Y + W\partial\xi/\partial Z + \xi(\partial U/\partial X + \partial V/\partial Y) \\ + (\partial W/\partial Y\cdot\partial U/\partial Z - \partial W/\partial X\cdot\partial V/\partial Z) \\ = \partial^2\xi/\partial X^2 + \partial^2\xi/\partial Y^2, \end{aligned} \tag{4}$$

$$\begin{aligned} U\partial W/\partial X + V\partial W/\partial Y + W\partial W/\partial Z \\ = -\mathrm{d}\overline{P}/\mathrm{d}Z + Ra/(Pr\cdot Re)\cdot(\theta-\theta_o)/(1-\theta_o) \\ + \partial^2 W/\partial X^2 + \partial^2 W/\partial Y^2, \end{aligned} \tag{5}$$

$$\begin{aligned} U\partial\theta/\partial X + V\partial\theta/\partial Y + W\partial\theta/\partial Z \\ = [\partial^2\theta/\partial X^2 + \partial^2\theta/\partial Y^2 + (1-\omega)\tau^2/N_c \\ \cdot(G^* - \theta^4)]/Pr. \end{aligned} \tag{6}$$

In the above formulation, the dimensionless groups are defined as follows:

$$\begin{aligned} &X = x/a, && Y = y/a, \\ &Z = z/(a\cdot Re), && U = ua/v, \\ &V = va/v, && W = w/w_o, \\ &\overline{P} = \overline{p}/(\rho w_o^2), && \theta = T/T_w, \\ &\theta_o = T_o/T_w, && Re = w_o a/v, \\ &Pr = v/\alpha, && Gr = g\beta(T_w - T_o)a^3/v^2, \\ &N_c = k\kappa/(4\overline{n}^2\sigma T_w^3), && \tau = \kappa a, \\ &\omega = \kappa_S/\kappa, && G^* = G/(\overline{n}^2\sigma T_w^4), \\ &Ra = Pr\cdot Gr, && Z^* = Z/Pr. \end{aligned} \tag{7}$$

The overall mass flow rate at every axial location must be balanced in the duct flow, i.e.,

$$\int_0^1\int_0^1 W\,\mathrm{d}X\mathrm{d}Y = 1. \tag{8}$$

For the radiation part of this problem, we consider a gray, absorbing and scattering medium. The radiation transfer equation is given in the dimensionless form as

$$\begin{aligned} \mu\partial\psi/\partial X + \eta\partial\psi/\partial Y + \tau\psi \\ = (1-\omega)\tau\theta^4 + \frac{\omega\tau}{4\pi}\int_{\Omega'=4\pi}\phi(\vec{\Omega}',\vec{\Omega})\psi\,\mathrm{d}\Omega', \end{aligned} \tag{9}$$

where the term $\partial\psi/\partial Z$ is omitted under the assumption of negligible axial radiation, i.e., $\partial q_{rz}/\partial Z \ll \partial q_{rx}/\partial X + \partial q_{ry}/\partial Y$. This assumption has been corroborated independently by Echigo et al. [20] and Campo and Schuler [23] who showed that the axial radiation penetrates one or two diameters upstream of the origin of the heat exchange section. In a dimensionless form, this penetrated distance is about $Z^* = 0.001$ for the flow with $Re = 2000$ in this work. Therefore, the axial radiation is discarded. In Eq. (9), $\psi = \pi I/(\overline{n}^2\sigma T_w^4)$ is the dimensionless intensity of radiation at a point (X, Y) in the direction $\vec{\Omega}$ defined by the direction cosines μ, η, and ζ, ω is the single scattering albedo, and $\phi(\vec{\Omega}', \vec{\Omega})$ is the scattering phase function, which is expressed in terms of Legendre polynomials as

$$\phi(\vec{\Omega}',\vec{\Omega}) = \sum_{n=0}^{N^*} a_n P_n(\mu'\mu + \eta'\eta + \zeta'\zeta). \tag{10}$$

If the surface is assumed to be opaque, gray and diffusely reflecting, the wall of boundary condition can be written as

$$\begin{aligned} \psi_w(\vec{\Omega}) = \epsilon_w + \frac{(1-\epsilon_w)}{\pi}\int_{\vec{n}\cdot\vec{\Omega}'<o} |\,\vec{n}\cdot\vec{\Omega}' \\ |\,\psi_w(\vec{\Omega}')\,\mathrm{d}\Omega', \quad \vec{n}\cdot\vec{\Omega} > 0, \end{aligned} \tag{11}$$

where ϵ_w is the wall emissivity, and $\vec{n}$ is the unit normal vector pointing out of the duct wall into the medium.

Once the dimensionless radiation intensity ψ is known, the dimensionless radiation flux vector and incident radiation are found from

$$\vec{Q}_r = \vec{q}_r/(4\bar{n}^2\sigma T_w^4) = (1/4\pi)\cdot\int_{\Omega=4\pi}\vec{\Omega}\psi\,d\Omega, \tag{12}$$

$$G^* = G/(4\bar{n}^2\sigma T_w^4) = (1/4\pi)\cdot\int_{\Omega=4\pi}\psi\,d\Omega. \tag{13}$$

The boundary conditions for the convective governing equations are

$$U = V = W = 0, \quad \theta = 1 \text{ at the duct walls,} \tag{14}$$

$$W = 1, \quad U = V = \xi = 0, \quad \theta = \theta_o \text{ at the entrance } Z = 0. \tag{15}$$

After the velocity and temperature fields are obtained, computation of the circumferentially averaged friction factor and Nusselt number is of practical interest. The dimensionless friction factor is

$$fRe = 2(\overline{\partial W/\partial n})_w. \tag{16}$$

Energy transport from the duct wall to the gas flow in the presence of thermal radiation depends on two related factors: The fluid temperature gradient on the duct wall and the rate of radiative heat exchange.

$$q_t = q_c + q_r = -k(\partial T/\partial n)_w + q_r. \tag{17}$$

The local total Nusselt number Nu_t defined as

$$Nu_t = \bar{h}a/k = q_t a/[k(T_w - T_b)], \tag{18}$$

consists of both convection and radiation heat transfer rates. It is written as

$$Nu_t = Nu_c + Nu_r, \tag{19}$$

where Nu_c and Nu_r are respectively, the local convective Nusselt number and radiative Nusselt number, and are defined as

$$Nu_c = -(\overline{\partial\theta_w/\partial n})/(1-\theta_b) \tag{20}$$

and

$$Nu_r = (\tau\bar{Q}_r/N_c)/(1-\theta_b), \tag{21}$$

where the overbar means the circumferential average, $\overline{Q_r}$ is the dimensionless radiative hear flux at the duct wall, and the bulk temperature θ_b is

$$\theta_b = \int_0^1\int_0^1 \theta\cdot W\,dX dY. \tag{22}$$

The parameters involved are the Prandtl number Pr, the ratio of the Rayleigh to Reynolds numbers, Ra/Re, the conduction-to-radiation N_c, the optical thickness τ, the scattering albedo ω, the wall emissivity ϵ_w and temperature ratio of inlet fluid and wall θ_o. The Ra/Re measures the importance of the thermal buoyancy effects relative to the inertia force. The conduction-to-radiation parameter N_c characterizes the relative importance with respect to radiation. The effect of radiation is getting strong as N_c decreases. To reduce the computational effort, the temperature ratio of inlet fluid and wall is fixed to be $\theta_o = 0.3$ and the Prandtl number is set to be $Pr = 0.7$. Effects of other parameters are examined in detail.

3. Solution method

The governing equations are solved numerically by the vorticity–velocity method for three-dimensional parabolic flow [25,26]. For a given combination of parameters, the field solutions are calculated by a marching technique based on the Du Fort–Frankel scheme [27]. Details of the solution procedure have been described elsewhere [25,26] and are not repeated herein. In the present work, the radiative transfer equation is solved by the discrete ordinates method with S_N quadrature [28–30]. The solid angle 4π is discretized over a finite number of directions, the radiative transfer equation is applied at these directions with the integral term replaced by a quadrature. The discrete ordinates representation of the radiative transfer equation is

$$\mu_m\partial\psi_m/\partial X + \eta_m\partial\psi_m/\partial Y + \tau\psi_m = (1-\omega)\tau\theta^4 + \frac{\omega\tau}{4\pi}\sum_{m'} w^*_{m'}\phi_{m'm}\psi_{m'}, \tag{23}$$

where subscripts m and m' represent the directions of the discrete ordinates, and the w^*_m are the quadrature weights. The associated boundary conditions are

$$\psi_m = \epsilon_w + \frac{(1-\epsilon_w)}{\pi}\sum_{m'}\psi_{m'} \mid \mu_{m'} \mid w^*_{m'}, \quad \mu_m > 0,\ \mu_m < 0,\ X = 0, \tag{24}$$

$$\psi_m = \epsilon_w + \frac{(1-\epsilon_w)}{\pi}\sum_{m'}\psi_{m'} \mid \mu_{m'} \mid w^*_{m'}, \quad \mu_m < 0,\ \mu_{m'} > 0,\ X = 1, \tag{25}$$

$$\psi_m = \epsilon_w + \frac{(1-\epsilon_w)}{\pi}\sum_{m'}\psi_{m'} \mid \mu_{m'} \mid w^*_{m'}, \quad \eta_m > 0,\ \eta_{m'} < 0,\ Y = 0, \tag{26}$$

$$\psi_m = \epsilon_w + \frac{(1-\epsilon_w)}{\pi}\sum_{m'}\psi_{m'} \mid \mu_{m'} \mid w^*_{m'}, \quad \eta_m < 0,\ \eta_{m'} < 0,\ Y = 1. \tag{27}$$

The discrete form of the phase function $\phi_{m'm}$ is

$$\phi_{m'm} = \sum_{n=0}^{N^*} a_n P_n(\mu_{m'}\mu_m + \eta_{m'}\eta_m + \zeta_{m'}\zeta_m). \tag{28}$$

Table 1
The discrete directions and quadrature weights for the S_6 method (one octant only)

m	μ_m	η_m	ζ_m	w_m^*
1	0.948235	0.224556	0.224556	$\pi/6$
2	0.689048	0.689048	0.224556	$\pi/6$
3	0.224556	0.948235	0.224556	$\pi/6$
4	0.689048	0.224556	0.689048	$\pi/6$
5	0.224556	0.689048	0.689048	$\pi/6$
6	0.224556	0.224556	0.948235	$\pi/6$

Table 2
Comparisons of local Nu_t for various grid arrangements for $Ra/Re = 100, N_c = 0.05, \tau = 1, \omega = 0, \epsilon_w = 0.5$ and $\theta_o = 0.3$

$M \times N$ (ΔZ^*)	Z^*					
	0.001	0.005	0.01	0.05	0.1	0.3
51×51 (1×10^{-5}–5×10^{-4})	15.528	9.533	8.274	8.460	8.787	8.398
81×81 (1×10^{-5}–5×10^{-4})	15.232	9.428	8.275	8.456	8.732	8.408
51×51 (1×10^{-6}–5×10^{-4})	15.640	9.397	8.275	8.464	8.787	8.463
31×31 (1×10^{-5}–5×10^{-4})	17.241	9.484	8.265	8.442	8.790	8.608

The angular discretization transforms the integro-differential radiative transfer equation into a set of coupled partial differential equations. The discrete directions and quadrature weights used in this work are based on the momentum-matching technique [31], as listed in Table 1. The total number of discrete directions is 24 when the S_6 scheme is employed for a two-dimensional geometry.

To ensure the independence of the grid points used in this work, a numerical experiment was made on the grids in the cross-sectional plane ($M \times N$) and axial step size (ΔZ^*). In this study, grids were arranged to be uniform in the cross-sectional direction but non-uniformly distributed in the axial direction for the uneven variations of field properties in the entrance region. It is found, Table 2, that the deviations in local total Nusselt number Nu_t calculated with $M \times N = 51 \times 51$ and $81 \times 81 (\Delta Z^* = 1 \times 10^{-5}$–$5 \times 10^{-4})$ are always less than 2% for $Ra/Re = 100$, $N_c = 0.05, \tau = 1, \omega = 0$ and $\epsilon_w = 0.5$. Furthermore, the deviations in Nu_t calculated using $M \times N$ (ΔZ^*) $= 51 \times 51$ ($\Delta Z^* = 1 \times 10^{-6}$–$5 \times 10^{-4}$) and 51×51 ($\Delta Z^* = 1 \times 10^{-5}$–$5 \times 10^{-4}$) are all less than 2%. Accordingly, the computations involving a $M \times N$ (ΔZ^*) $= 51 \times 51$ ($\Delta Z^* = 1 \times 10^{-5}$–$5 \times 10^{-4}$) grid are considered to be sufficiently accurate to describe the flow and heat transfer in a vertical square duct. All the results presented in the next section are computed using the latter grid. As a partial verification of the computational procedure, results were initially obtained for convection heat transfer in a vertical square duct without thermal radiation effect and compared with those of Cheng and Weng [17]. The Nusselt number and friction factor were found to agree within 2%. Through these numerical tests, the present numerical scheme was suitable for the present problem.

4. Results and discussion

The developing axial velocity profiles along the centerlien $X = 0.5$ at various conditions are shown in Fig. 1, where curves A, B, C, D, and E denote profiles at $Z^* = 0.001, 0.01, 0.05, 0.1,$ and 0.3, respectively. For comparison, the results without thermal radiation effect are also included in Fig. 1, as indicated by the dashed lines. It should be mentioned that the uniform velocity at the entrance $Z = 0$ corresponds to $W = 1$ in these subplots. In the absence of buoyancy [see Fig. 1(b)], the W profiles change along the duct axis, beginning with a square shape at $Z = 0$ and finally taking a parabolic shape further downstream. Therefore, maximum velocity always occurs at the centerline of $Y = 0.5$. Once buoyancy is initiated, the W profiles may shift towards the duct walls ($Y = 0$ and 1), especially for the curves without radiation effect. Near the entrance (curve A), the velocity profile is fairly uniform over the cross-section. As the flow develops, the velocity in the core region is accelerated due to the entrance effect. Further downstream, the velocity profile becomes distorted with the maximum velocity towards the duct walls (curve C).

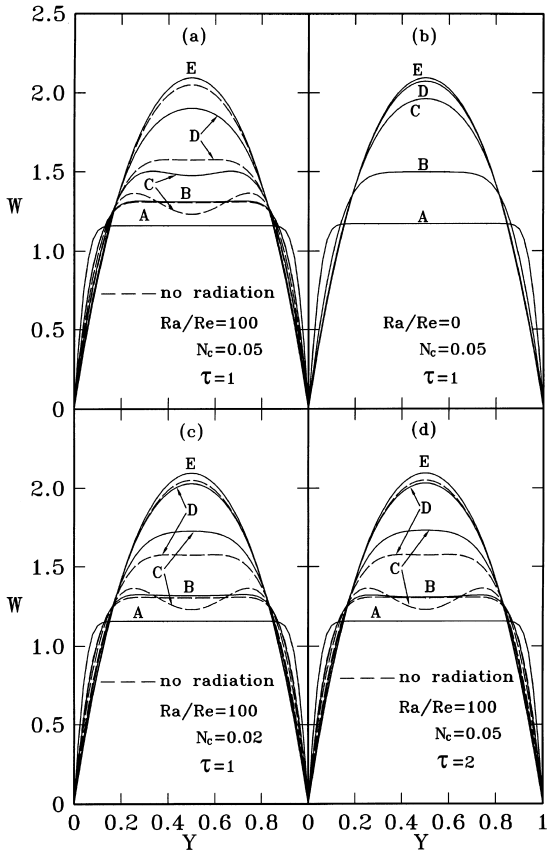

Fig. 1. Development of axial velocity profiles for different conditions: A: $Z^* = 0.001$, B: $Z^* = 0.01$, C: $Z^* = 0.05$, D: $Z^* = 0.1$, and E: $Z^* = 0.3$.

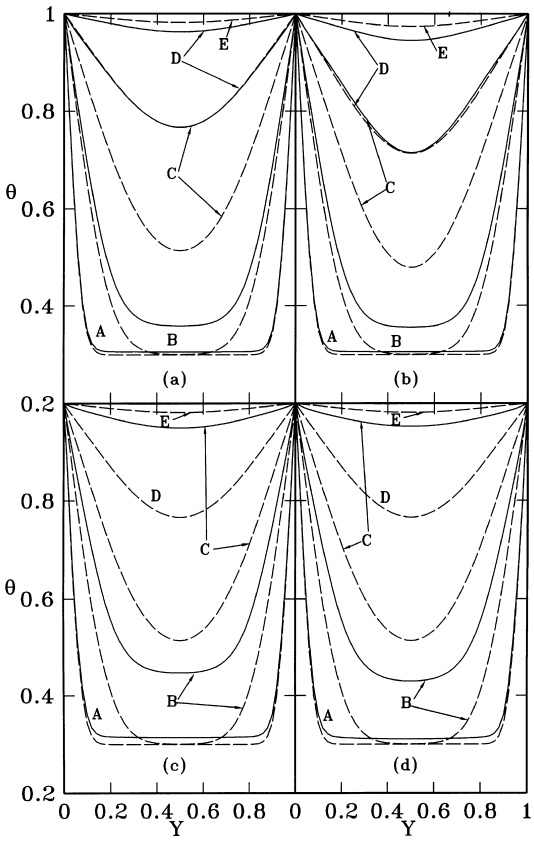

Fig. 2. Development of temperature profiles for different conditions: A: $Z^* = 0.001$, B: $Z^* = 0.01$, C: $Z^* = 0.05$, D: $Z^* = 0.1$ and E: $Z^* = 0.3$.

Finally, the velocity profiles become parabolic when the flow is fully developed. But as the radiation effect is taken into account (shown by the solid curves), the radiation tends to reduce the buoyancy effects. Therefore, the extent of the velocity shifting towards the walls becomes less significant, especially for stronger radiation cases (e.g., smaller N_c or larger τ). This can be understood by recognizing that the radiative heat flux is an additional mode of energy transport that causes a flatter temperature distribution. This world cause a small buoyancy effect. A close inspection of the solid and dashed curves discloses that the radiation effect tends to reduce W near the walls ($Y = 0$ and $Y = 1$). This implies that the results with radiation would reduce the friction factor.

Plotted in Fig. 2 are the temperature profiles at different axial locations, with the same legends as Fig. 1. In line with the wall heating, the temperature in the central portion of the duct increases gradually as the flow moves downstream. A comparison of the temperature profiles with and without radiation reveals that near the inlet the effect of radiation on the thermal development is insignificant. But at the downstream location, radiation effect tends to equalize the temperature in the flow. A close inspection of Fig. 2(a) and (c) shows that as the condition-to-radiation parameter N_c decreases, the θ becomes flatter. Additionally, the development of temperature profile is faster for a system with a stronger radiation effect ($N_c = 0.02$). This can be understood by recognizing that the radiative heat flux is an additional mode of energy transport and as the magnitude of N_c decreases, the importance of the radiation term in Eq. (6) increases, relative to the conduction and convection. This causes an increase of the energy transport which leads to flatter temperature profiles. Similar result is also found for the case with a large τ.

The effects of the ratio of Rayleigh number to Reynolds number Ra/Re and conduction-to-radiation parameter N_c on the axial variations of bulk temperature θ_b are presented in Fig. 3. For comparison purposes, the results without thermal radiation effect are also plotted in Fig. 3, as shown by the dashed lines. It is clear that due to the stronger buoyancy effects, the development of bulk temperature is quicker for a sys-

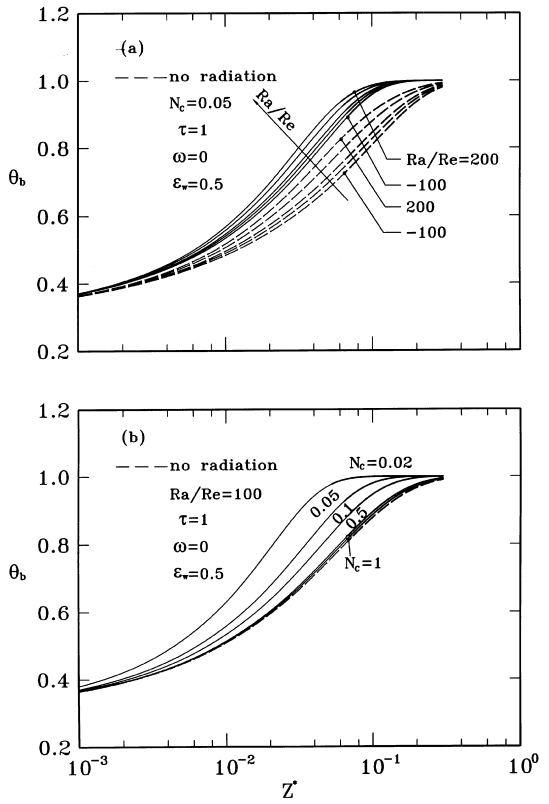

Fig. 3. Effects of Ra/Re and N_c on the axial variation of the bulk temperature θ_b for $\tau = 1$, $\omega = 0$ and $\epsilon_w = 0.5$.

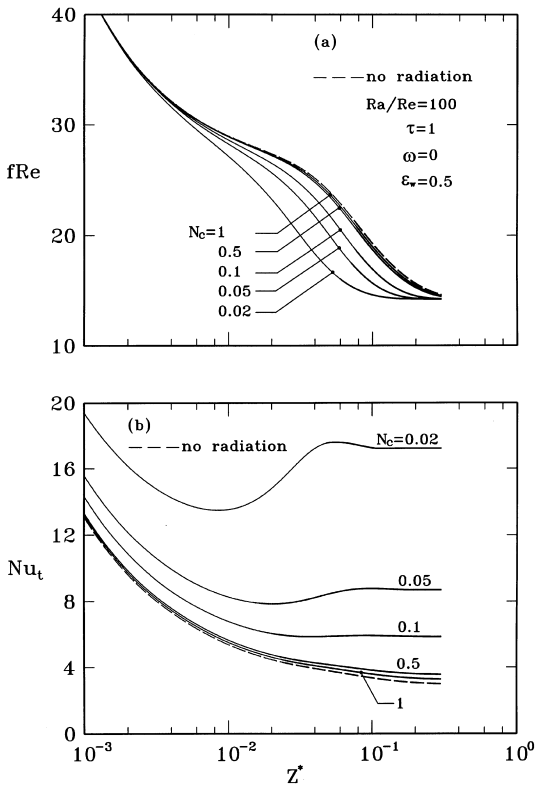

Fig. 4. Effects of N_c on the variation of the friction factor and the Nusselt number for $Ra/Re = 100$, $\tau = 1$, $\omega = 0$ and $\epsilon_w = 0.5$.

tem with a larger Ra/Re. In addition, the θ_b is found to be essentially the same as that without radiation when the radiation-convection interaction is weak, such as for the curve of $N_c = 1$. However, when the interaction is intense ($N_c = 0.02$), there is an essential difference. In contrast to the case without radiation, the radiation augments the rate of thermal development so that the θ_b approaches the wall temperature ($\theta = 1$) at a more rapid rate.

The effects of the conduction-to-radiation parameter N_c on the axial variations of local friction factor and Nusselt number are presented in Fig. 4. In Fig. 4, the total Nusselt number Nu_t with radiation is larger than that without radiation. This is due to two effects. The first is that radiation is an additional mechanism for heat transfer through the fluid, resulting in an increased heat flux. Secondly, the radiation source term augments the rate of thermal development so that the bulk temperature approaches the wall temperature at a more rapid rate. Both effects act to increase the local total Nusselt number Nu_t. Near the entrance, the Nu_t is raised only by the additional radiative heat flux, while further downstream, the more rapid thermal development contributes when the bulk temperature approaches the wall temperature. An overall inspection of Fig. 4 reveals that near the entrance, the local fRe fades away monotonically due to the entrance effect. And at these positions, the convective effect is predominant. Therefore, the effects of N_c on the local fRe are insignificant. But as the flow proceeds downstream, the radiation effect becomes important. The fRe decreases with a decrease in N_c. This is due to the fact that in the presence of radiation, the temperature field becomes flatter, as shown in Fig. 2. The buoyancy-assisting effect is thus reduced, which in turn, causes a reduction in fRe further downstream. But this is not the case with the local Nu_t. At downstream region, the Nu_t increases with a decrease in N_c due to the strong radiation effect.

The optical thickness τ is another important factor which affects the heat transfer and fluid flow. Fig. 5 shows the effects of optical thickness τ on the local fRe and Nu_t. When τ is very small, the medium is almost transparent. Thus, it does not absorb and emit much energy. A large τ corresponds to a strong radiatively participating medium. It is easy to see that there is more heat released from such a medium than from a weak radiatively participating medium. Thus, the local Nu_t increases with an increases in τ. Additionally, the

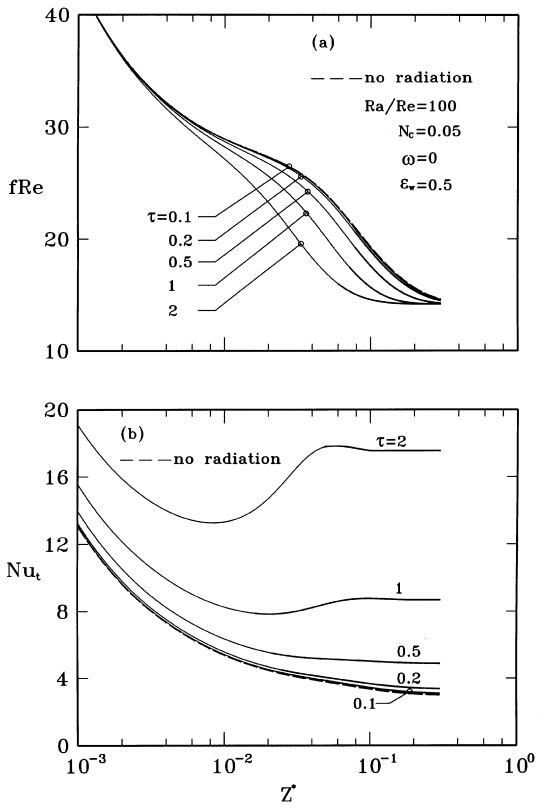

Fig. 5. Effects of τ on the variation of the friction factor and the Nusselt number for $Ra/Re = 100$, $N_c = 0.05$, $\omega = 0$ and $\epsilon_w = 0.5$.

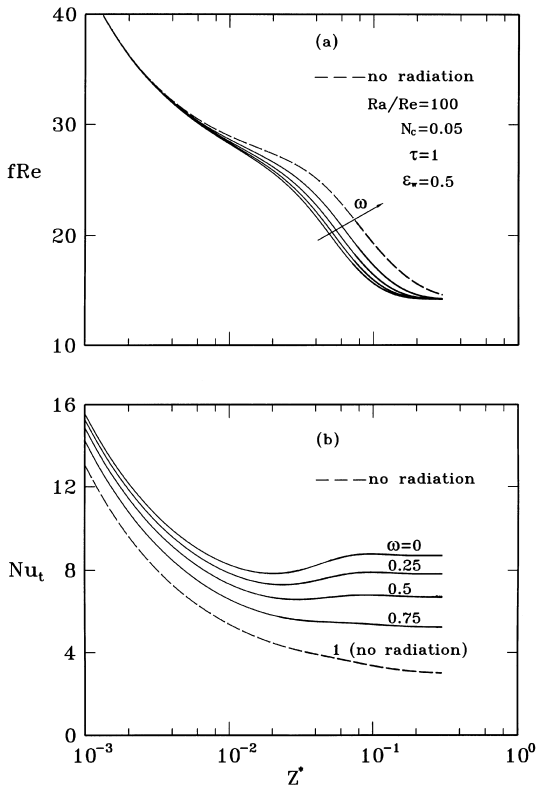

Fig. 6. Effects of ω on the variation of the friction factor and the Nusselt number for $Ra/Re = 100$, $N_c = 0.05$, $\tau = 1$ and $\epsilon_w = 0.5$.

radiation has a stronger effect on the local fRe and Nu_t for a system with a larger τ, as compared with the results of no radiation.

In many applications, scattering processes are important in radiative heat transfer if particulates are present in the fluid. Therefore, the effects of the single scattering albedo on the fluid flow and heat transfer are of interest. For illustration, the scattering is assumed to be isotropic. Fig. 6 demonstrates the influence of scattering albedo ω on the local fRe and Nu_t distributions. The Nu_t decreases with the increasing single scattering albedo ω. This is expected, since as the scattering albedo ω approaches zero, the emission and absorption of energy within the medium dominate. As the scattering albedo ω approaches unity, scattering dominates and causes a small Nu_t. Like the results in Fig. 5(a), the local fRe is attenuated due to the radiation effect in the downstream region.

The effects of wall emissivity ϵ_w on the local fRe and Nu_t are shown in Fig. 7. It is apparent that the local Nu_t without radiation is lower than that with radiation. Additionally, the local Nu_t increases with the increasing emissivity of the duct wall. Naturally, heat transfer is maximum for a black duct (i.e., $\epsilon_w = 1$). It is also found that the stronger the radiation effect, the smaller the fRe.

In the conditions of high wall-to-coolant temperature differences, buoyancy may play a very critical role in the flow and heat transfer mechanism. Hence, it is interesting to examine its influence on the flow and heat transfer. Fig. 8 shows the effects of the Ra/Re on the local fRe and Nu_t for $N_c = 0.05$, $\tau = 1$, $\omega = 0$ and $\epsilon_w = 0.5$. Positive Ra/Re indicates a buoyancy-assisting flow, while negative Ra/Re means a buoyancy-opposing flow. It is obvious that the buoyancy-assisting effect increases the fRe and Nu_t as compared with the results of buoyancy-free case ($Ra/Re = 0$), and the extent of increase in Nu_t increases with the magnitude of Ra/Re. But for the case of negative Ra/Re, the opposing buoyancy decreases the local fRe and Nu_t. Additionally, relative to the results without radiation, the radiation effect would decrease the local fRe for the buoyancy-assisting case. But for buoyancy-opposing flow, the presence of radiation would enhance the local fRe. These are due to the fact that the radiation tends to reduce the buoyancy effects.

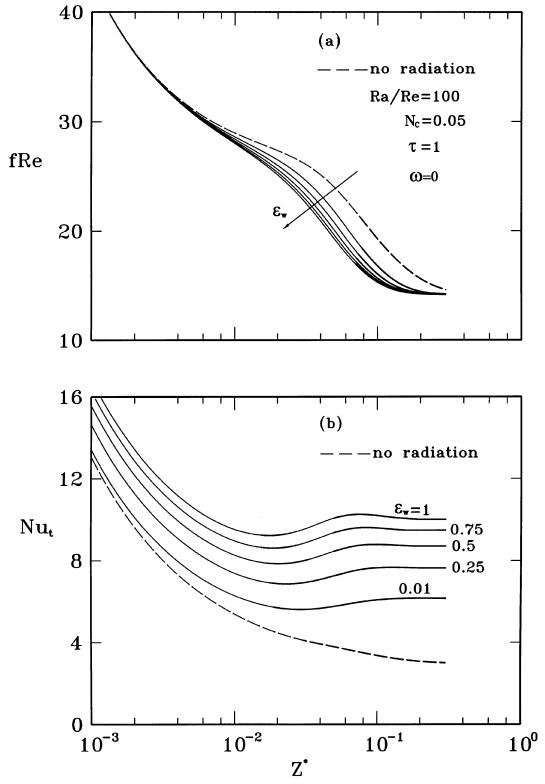

Fig. 7. Effects of ϵ_w on the variation of the friction factor and the Nusselt number for $Ra/Re = 100$, $N_c = 0.05$, $\tau = 1$ and $\omega = 0$.

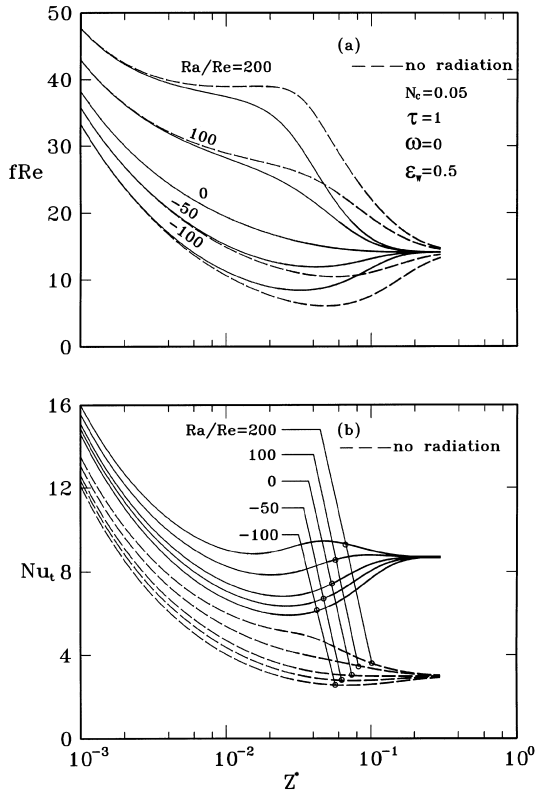

Fig. 8. Effects of Ra/Re on the variation of the friction factor and the Nusselt number for $N_c = 0.05$, $\tau = 1$, $\omega = 0$ and $\epsilon_w = 0.5$.

5. Conclusions

In the present work, the problem of mixed convection flow and heat transfer in a vertical square duct with consideration of thermal radiation has been studied numerically. A novel vorticity–velocity method successively solved the three-dimensional parabolic governing equations. The radiative transfer equation was solved by the discrete ordinates method. The effects of the Rayleigh number-to-Reynolds number parameter Ra/Re, conduction-to-radiation parameter N_c, optical thickness τ, single scattering albedo ω and wall emissivity ϵ_w on the flow and heat transfer are examined in detail. What follows is a brief summary.

1. In the presence of radiation, the thermal development develops at a more rapid rate relative to that without radiation.
2. The local friction factor fRe and Nusselt number Nu_t are enhanced with an increase in the magnitude of Ra/Re for buoyancy-assisting case.
3. The local total Nusselt number Nu_t is augmented by the radiation effects. The fRe is reduced (increased) for the buoyancy-assisting (opposing) flow as the thermal radiation effect is taken into account.
4. In contrast to the results without radiation, radiation effects augment the Nu_t. And the extent of enhancement in Nu_t increases with a decrease (increase) in N_c or ω (τ or ϵ_w).
5. The laminar case is treated in this work and intended to provide a first step towards future work which will investigate the radiation effects on turbulent mixed convection in vertical ducts.

Acknowledgements

The financial support of this research by the National Science Council under the contract NSC 87-2212-E-211-006 is greatly appreciated. The authors wish to thank the referees for their suggestions and criticisms which contributed to improve the quality of the present article.

References

[1] J.D. Jackson, M.A. Cotton, B.P. Axcell, Studies of mixed convection in a vertical tube: review, Int. J. Heat Fluid Flow 10 (1989) 2–15.

[2] W. Aung, G. Worku, Developing flow and flow reversal in a vertical channel with asymmetric wall temperatures, ASME J. Heat Transfer 108 (1986) 299–304.
[3] W. Aung, G. Worku, Theory of fully developed combined convection including flow reversal, ASME J. Transfer 108 (1986) 485–488.
[4] W. Aung, G. Worku, Mixed convection in ducts with asymmetric wall heat fluxes, ASME J. Heat Transfer 109 (1987) 947–951.
[5] S. Habchi, S. Acharya, Laminar mixed convection in a asymmetrically or symmetrically heated vertical channel, Numer. Heat Transfer 9 (1986) 605–618.
[6] C. Gau, K.A. Yih, W. Aung, Measurements of heat transfer and flow structure in vertical channels, AIAA J. Thermophys. Heat Transfer 6 (1992) 707–712.
[7] D.B. Ingham, D.J. Keen, P.J. Heggs, Two-dimensional combined convection in vertical parallel plate ducts, Internat. J. Numer. Methods Engrg. 26 (1988) 1645–1664.
[8] D.B. Ingham, D.J. Keen, P.J. Heggs, Flows in vertical channels with asymmetric wall temperatures and including situations where reverse flow occurs, ASME J. Heat Transfer 110 (1999) 910–917.
[9] C. Gau, K.A. Yih, W. Aung, Reversal flow structure and heat transfer measurement for buoyancy-assisted convection in a heated vertical duct, ASME J. Heat Transfer 114 (1992) 928–935.
[10] Y.N. Jeng, J.L. Chen, W. Aung, On the Reynolds-number independence of mixed convection in a vertical channel subjected to asymmetric wall temperature with and without flow reversal, Int. J. Heat Fluid Flow 13 (1992) 329–339.
[11] T.F. Lin, T.S. Chang, Y.F. Chen, Development of oscillatory asymmetric recirculating flow in transient laminar opposing mixed convection in symmetrically heated vertical channel, ASME J. Heat Transfer 105 (1993) 342–352.
[12] P.J. Hegg, D.B. Ingham, D.J. Keen, The effects of heated conduction in the wall on the development of recirculating combined convection flows in vertical tubes, Int. J. Heat Mass transfer 33 (1990) 517–528.
[13] M. Wang, T. Tsuji, Y. Nagano, Mixed convection with flow reversal in the thermal entrance region of horizontal and vertical pipes, Int. J. Heat Mass Transfer 37 (1994) 2305–2319.
[14] H. Hesreddin, N. Galanis, C.T. Nguyen, Effects of axial diffusion on laminar heat transfer with low Peclet numbers in the entrance region of thin vertical tubes, Numer. Heat Transfer Part A 33 (1998) 247–266.
[15] M. Igbal, B.D. Aggarwala, Combined free and forced convection through vertical rectangular channels with unequal heating from sides, J. Appl. Mech. (1971) 829–833.
[16] C.H. Cheng, C.J. Weng, Flow reversal of combined convection in a vertical rectangular duct with unequally isothermal walls, Int. Commu. Heat Mass Transfer 18 (1991) 127–140.
[17] C.H. Cheng, C.J. Weng, Developing flow of mixed convection in a vertical rectangular duct with one heating wall, Numer. Heat Transfer Part A 24 (1993) 479–493.
[18] J.C. Chen, Laminar heat transfer in a tube with nonlinear radiant heat-flux boundary conditions, Int. J. Heat Mass Transfer 9 (1966) 433–440.
[19] B.E. Pearce, A.F. Emery, Heat transfer by thermal radiation and laminar forced convection to an absorbing fluid in the entry region of a pipe, ASME J. Heat Transfer 92 (1970) 221–230.
[20] R. Echigo, S. Hasegawa, K. Kamiuto, Composite heat transfer in a pipe with thermal radiation of two-dimensional propagation in connection with the temperature rise in a flowing medium upstream of a heating section, Int. J. Heat Mass Transfer 18 (1975) 1149–1159.
[21] A.T. Wassel, D.K. Edwards, Molecular radiation in a laminar or turbulent pipe flow, ASME J. Heat Transfer 98 (1976) 101–107.
[22] F.H. Azad, M.F. Modest, Combined radiation and convection in absorbing emitting and anisotropically scattering gas-particulate tube flow, Int. J. Heat Mass Transfer 24 (1981) 1681–1697.
[23] A. Campo, C. Schuler, Thermal radiation and laminar forced convection in a gas pipe flow, Warme- und Stoffubertraggung 22 (1988) 251–257.
[24] T. Seo, D.A. Kaminski, M.K. Jensen, Combined convection and radiation in simultaneously developing flow and heat transfer with nongray gas mixtures, Numer. Heat Transfer Part A 26 (1994) 49–66.
[25] K. Ramakrishna, S.G. Rubin, P.K. Khosla, Laminar natural convection along vertical square ducts, Numer. Heat Transfer 5 (1982) 59–79.
[26] W.M. Yan, C.Y. Soong, Simultaneously developing mixed convection in radially rotating rectangular ducts, Int. J. Heat Mass Transfer 38 (1995) 665–677.
[27] P.J. Roche, Computational Fluid Dynamics, Reinhold, New York, 1971, pp. 61–64.
[28] W.A. Fiveland, Three-dimensional radiative heat transfer solution by the discrete-ordinates method, J. Thermophys. Heat Transfer 2 (1988) 309–316.
[29] T.Y. Kim, S.W. Baek, Analysis of combined conductive and radiative heat transfer in a two-dimensional rectangular enclosure using the discrete ordinates method, Int. J. Heat Mass Transfer (1991) 2265–2273.
[30] M.F. Modest, Radiative Heat Transfer, McGraw-Hill, New York, 1993, pp. 541–571.
[31] B.G. Carlson, K.D. Lathrop, Transport theory: the method of discrete ordinates, in: H. Greenspan, C.N. Kelber, D. Okrent (Eds.), Computing Methods in Reactor Physics, Gordon & Breach, New York, 1968, pp. 165–266.